FERMILAB-PUB-22-391-T

Prepared for submission to JCAP

Constraining the Milky Way's Pulsar Population with the Cosmic-Ray Positron Fraction

Olivia Meredith Bitter[a,b] **and Dan Hooper**[a,b,c]

[a]Fermi National Accelerator Laboratory, Batavia, IL 60510
[b]University of Chicago, Chicago, IL 60637
[c]University of Chicago, Kavli Institute for Cosmological Physics, Chicago, IL 60637

E-mail: obitter16@uchicago.com, orcid.org/0000-0002-0600-9095,
dhooper@fnal.gov, orcid.org/0000-0001-8837-4127

Abstract. Observations of the TeV halos associated with nearby pulsars indicate that these objects inject significant fluxes of very high-energy electron-positrons pairs into the interstellar medium (ISM), thereby likely providing the dominant contribution to the cosmic-ray positron flux. In this paper, we use the cosmic-ray positron fraction as measured by the AMS-02 Collaboration to constrain the characteristics of the local pulsar population. For reasonable model parameters, we find that we can obtain good agreement with the measured positron fraction up to energies of $E_e \sim 300\,\text{GeV}$. At higher energies, the positron fraction is dominated by a small number of pulsars, making it difficult to reliably predict the shape of the expected positron fraction. The low-energy positron spectrum supports the conclusion that pulsars typically transfer approximately $\eta \sim 5-20\%$ of their total spindown power into the production of very high-energy electron-positron pairs, producing a spectrum of such particles with a hard spectral index, $\alpha \sim 1.5-1.7$. Such pulsars typically spindown on a timescale on the order of $\tau \sim 10^4\,\text{years}$. Our best fits were obtained for models in which the radio and gamma-ray beams from pulsars are detectable to 28% and 62% of surrounding observers, respectively.

This manuscript has been authored by Fermi Research Alliance, LLC under Contract No. DE-AC02-07CH11359 with the U.S. Department of Energy, Office of Science, Office of High Energy Physics.

Contents

1 Introduction

Recent observations by the HAWC Collaboration [8, 1, 2, 7] indicate that young and middle-aged pulsars (and also possibly millisecond pulsars [15, 18]) produce significant fluxes of very high-energy gamma rays through the inverse Compton scattering of electrons and positrons [19, 22, 28, 29]. This emission leads to the appearance of "TeV halos" surrounding most, if not all, pulsars. Furthermore, the observed characteristics of these TeV halos support the conclusion that these sources are likely responsible for the cosmic-ray positron excess [19, 16] reported by the AMS-02 Collaboration [30], and previously by PAMELA [3], AMS-01 [4], and HEAT [9] (for earlier work, see Refs. [10, 27]).

In early work, discussions of TeV halos in relation to the cosmic-ray positron fraction tended to focus on the contributions from a small number of nearby and high-spindown power pulsars, such as Geminga and Monogem [19, 21, 14]. It has since become clear, however, that the positrons detected by AMS do not originate from only a few pulsars. Instead, the cosmic-ray positron fraction receives substantial contributions from a significant number of such objects found throughout the surrounding kiloparsecs of the Milky Way [12, 26].

In this paper, we revisit TeV halos as a source of cosmic-ray positrons, using the measured characteristics of the cosmic-ray positron fraction to constrain the properties of the local pulsar population. Toward this goal, we have calculated the cosmic-ray positron flux from the known pulsars contained within the Australia Telescope National Facility (ATNF) pulsar catalog [24], taking into account the effects of diffusion, inverse Compton scattering, and synchrotron. We then accounted for those nearby pulsars which have thus far gone undetected, employing a Monte Carlo to simulate this population of sources. Using this Monte Carlo, we have calculated the contribution to the cosmic-ray positron flux from these pulsars, and compared these results to the positron fraction as reported by AMS-02, varying a variety of parameters including the spectral shape of the injected positrons, the timescale for pulsar spindown, the efficiency for electron-positron production, the magnitude of the magnetic field in the interstellar medium (ISM), and the duration of these objects' pulsar wind nebula phase.

For reasonable choices of these parameters, we have found that it is possible to obtain good agreement with the measured positron fraction, at least up to energies of $E_e \sim 300\,\mathrm{GeV}$. This result supports the conclusion that pulsars and their associated TeV halos are likely to be the dominant source of the observed cosmic-ray positron spectrum. At energies above a few hundred GeV, the positron fraction is dominated by a small number of pulsars, making it difficult to reliably predict the shape of the expected positron fraction or to use this high-energy information to draw reliable conclusions pertaining to the Milky Way's broader pulsar population. The low energy spectrum supports a picture in which pulsars typically transfer approximately $\eta \sim 5-20\%$ of their total spindown power into the production of high-energy electron-positron pairs, producing a spectrum of such particles with a hard spectral index, $\alpha \sim 1.5-1.7$. Such pulsars typically spindown on a timescale on the order of $\tau \sim 10^4$ years. Our best fits were obtained for models in which the radio and gamma-ray beams from pulsars are detectable to 28% and 62% of all surrounding observers, respectively.

2 Pulsars as a Source of High-Energy Positrons

Once a high-energy electron or positron has escaped from a TeV halo, their transport through the ISM is described by the following diffusion-loss equation:

$$\frac{\partial}{\partial t}\frac{dn_e}{dE_e}(E_e,r,t) = \vec{\nabla}\cdot\left[D(E_e)\vec{\nabla}\frac{dn_e}{dE_e}(E_e,r,t)\right] + \frac{\partial}{\partial E_e}\left[\frac{dE_e}{dt}(E_e,r)\frac{dn_e}{dE_e}(E_e,r,t)\right] + \delta(r)Q(E_e,t), \tag{2.1}$$

where r is the distance from the pulsar, Q characterizes the spectrum and time profile of the injected particles, dn_e/dE_e is the electron and/or positron number density per unit energy, and E_e is the energy of the electrons and positrons. The normalization and energy dependence of the diffusion coefficient, D, is constrained by the measurements of various secondary-to-primary ratios in the cosmic-ray spectrum. Throughout this study we will adopt a parameterization given by $D = (2\times10^{28}\,\mathrm{cm^2/s})\,(E_e/\mathrm{GeV})^{0.4}$ [31, 17]. The energy losses of high-energy electrons and positrons are dominated by a combination of inverse Compton scattering and synchrotron processes, resulting in the following rate:

$$\begin{aligned} -\frac{dE_e}{dt}(E_e,r) &= \sum_i \frac{4}{3}\sigma_T\rho_i(r)S_i(E_e)\left(\frac{E_e}{m_e}\right)^2 + \frac{4}{3}\sigma_T\rho_{\rm mag}(r)\left(\frac{E_e}{m_e}\right)^2 \\ &\approx 1.02\times10^{-16}\,\mathrm{GeV/s}\left(\frac{E_e}{\mathrm{GeV}}\right)^2\times\left[\sum_i\frac{\rho_i(r)}{\mathrm{eV/cm^3}}S_i(E_e) + 0.224\left(\frac{B(r)}{3\,\mu\mathrm{G}}\right)^2\right], \end{aligned} \tag{2.2}$$

where the σ_T is the Thomson cross section, $\rho_{\rm mag} \approx 0.224\,\mathrm{eV/cm^3}\times(B_{\rm ISM}/3\,\mu\mathrm{G})^2$ is the energy density of the magnetic field, and the sum is performed over different components of the radiation field, consisting of the cosmic microwave background (CMB), infrared emission (IR), starlight (star), and ultraviolet emission (UV). Lastly, the quantity $S_i(E_e)$ is a factor that accounts for the Klein-Nishina suppression of the inverse Compton scattering cross section, and is given by

$$S_i(E_e) \approx \frac{45m_e^2/64\pi^2T_i^2}{(45m_e^2/64\pi^2T_i^2)+(E_e^2/m_e^2)}. \tag{2.3}$$

Throughout our analysis, we will follow Ref. [19] in adopting the following parameters for the radiation model: $\rho_{\rm CMB} = 0.260\,\mathrm{eV/cm^3}$, $\rho_{\rm IR} = 0.60\,\mathrm{eV/cm^3}$, $\rho_{\rm star} = 0.60\,\mathrm{eV/cm^3}$, $\rho_{\rm UV} =$

$0.10\,\mathrm{eV/cm^3}$, $T_{\rm CMB} = 2.7\,\mathrm{K}$, $T_{\rm IR} = 20\,\mathrm{K}$, $T_{\rm star} = 5000\,\mathrm{K}$, and $T_{\rm UV} = 20,000\,\mathrm{K}$. At very high energies ($E_e \gg m_e^2/T$), inverse Compton scattering is strongly Klein-Nishina suppressed. This is particularly important for the scattering of cosmic-ray electrons and positrons with UV and starlight photons.

For the time profile of the source term in Eq. 2.1, we assume that the rate at which high-energy positrons and electrons are injected from a pulsar into the ISM is proportional to the rate at which that pulsar is losing rotational kinetic energy (i.e. its spindown power). For the case of magnetic-dipole breaking, a pulsar's spindown power is given by

$$\begin{aligned} \dot{E}(t) &= -\frac{8\pi^4 B^2 R^6}{3c^3 P(t)^4} \\ &\approx 1.0 \times 10^{35}\,\mathrm{erg/s} \times \left(\frac{B}{1.6\,\times\,10^{12}\,\mathrm{G}}\right)^2 \left(\frac{R}{15\,\mathrm{km}}\right)^6 \left(\frac{0.23\,\mathrm{sec}}{P(t)}\right)^4, \end{aligned} \tag{2.4}$$

where B, R, and P are the pulsar's magnetic field, radius, and period. Solving this differential equation, we obtain the following expression for the time evolution of the pulsar's period:

$$P(t) = P_0 \left(1 + \frac{t}{\tau}\right)^{\frac{1}{2}}, \tag{2.5}$$

where P_0 is the pulsar's initial period and τ is the spindown timescale, given by

$$\begin{aligned} \tau &= \frac{3c^3 I P_0^2}{4\pi^2 B^2 R^6} \\ &\approx 9.1\,\times 10^3\,\mathrm{yr} \times \left(\frac{1.6 \times 10^{12}\,\mathrm{G}}{B}\right)^2 \left(\frac{M}{1.4\,M_\odot}\right) \left(\frac{15\,\mathrm{km}}{R}\right)^4 \left(\frac{P_0}{0.040\,\mathrm{sec}}\right)^2, \end{aligned} \tag{2.6}$$

where I and M are the moment of inertia and mass of the neutron star.

During a young neutron star's pulsar wind nebulae phase, positrons and electrons can be confined to the region surrounding the object. With this in mind, we set the positron and electron injection rate to zero prior to a time, $t_{\rm PWN}$, which we expect to be on the order of $\mathcal{O}(10^4\,\mathrm{yr})$.

To obtain the total source term, Q, we multiply the spindown power by a constant efficiency factor, η, and parameterize the spectral shape using a power-law with an exponential cutoff:

$$Q(E_e, t) = \begin{cases} 0, & t < t_{\rm PWN} \\ \eta\,\dot{E}(t)\,Q_0\,E^{-\alpha}\,e^{-E_e/E_c}, & t > t_{\rm PWN} \end{cases} \tag{2.7}$$

where the normalization coefficient, Q_0, is set such that η is equal to the fraction of the pulsar's spindown power that goes into the production of positrons and electrons with $E_e > 10\,\mathrm{GeV}$ (for all $t > t_{\rm PWN}$):

$$\eta = \frac{\int_{10\,\mathrm{GeV}} Q(E_e, t)\,E_e\,dE_e}{\dot{E}(t)}. \tag{2.8}$$

Putting this together, we solve the diffusion-loss equation as described in Ref. [19] to find the spectrum of electrons and positrons from a given pulsar at the location of the

Solar System. The resulting positron spectrum depends on many parameters, including the distance to the pulsar, the pulsar's age, spindown timescale, initial period, and efficiency, as well as the duration of the pulsar wind nebula phase, the magnitude of the magnetic field in the ISM, and the spectral index and cutoff energy of the injected spectrum.

Once we have calculated the spectrum of positrons and electrons from the pulsars under consideration, we can combine this information with the spectrum of additional primary electrons (such as those from supernova remnants), as well as the spectra of secondary positrons and electrons that are produced through the propagation of primary cosmic rays. Taken together, this can be used to calculate the cosmic-ray positron fraction, defined as the positron flux divided by the combined flux of electrons and positrons. In calculating the positron fraction, we use the secondary spectra as obtained using the publicly available code GALPROP[1], and fix the primary spectrum using the measured cosmic-ray electron spectrum, assuming that pulsars produce an identical spectrum of positrons and electrons [25, 31]. To account for the finite energy resolution of AMS-02, we convolve the spectrum we calculate in each case with a Gaussian of width $\sigma = 0.02\, E_e$ [30].

3 Positrons From Known Pulsars

We begin our analysis by calculating the contribution to the cosmic-ray positron flux from known pulsars; namely those contained within the Australia Telescope National Facility (ATNF) pulsar catalog [24]. To this end, we consider the 103 ANTF pulsars that are located within 3 kpc of the Solar System and that are younger than $\tau_c < 10^6$ years.[2]

In Fig. 1, we plot the contribution to the cosmic-ray positron fraction from each of these 103 pulsars (thin colored lines), and from the sum of all 103 of these sources (thick black line), and compare this to the spectrum measured by the AMS-02 Collaboration [5, 6, 13]. Here, we have adopted the following parameters: $\alpha = 1.5$, $E_c = 50\,\text{TeV}$, $\eta = 0.15$, $\tau = 10^4\,\text{yr}$, $B_{\rm ISM} = 3\,\mu\text{G}$, and $t_{\rm PWN} = 3 \times 10^4\,\text{yr}$. For each individual pulsar, we adopt values of τ_c, r, and P as reported in the ATNF catalog (see Table 1). Keep in mind that this figure only reflects the contributions to the cosmic-ray positron flux from those pulsars contained in the ATNF catalog, which is largely limited to relatively young sources with radio or gamma-ray beams pointed in the direction of the Solar System.

The locations of the peaks that appear in the spectrum shown in Fig. 1 correspond to the energies to which very high-energy positrons can cool in an amount of time equal to the age of the pulsar in question [19]. For this reason, the older pulsars in this sample tend to exhibit spectral features which peak at relatively low energies. This opens the possibility that individual pulsars could generate distinctive spectral features in the positron spectrum. Conversely, the lack of such features could be used to constrain the characteristics of such pulsars [11].

It is interesting to note that the Geminga and Monogem pulsars are responsible for only a modest fraction of the total local positron flux. More specifically, while the contribution from Geminga (PSR J0633+1746, shown in light green in Fig. 1) is among the largest from these pulsars, the positron flux from Monogem does not even make the list of sources presented in Table 1.

[1] http://galprop.stanford.edu/.

[2] The characteristic age of a pulsar is defined by $\tau_c \equiv P/2\dot{P}$. For the case of magnetic dipole braking, this is related to a pulsar's true age, t, and spindown timescale according to $t = \tau_c - \tau$.

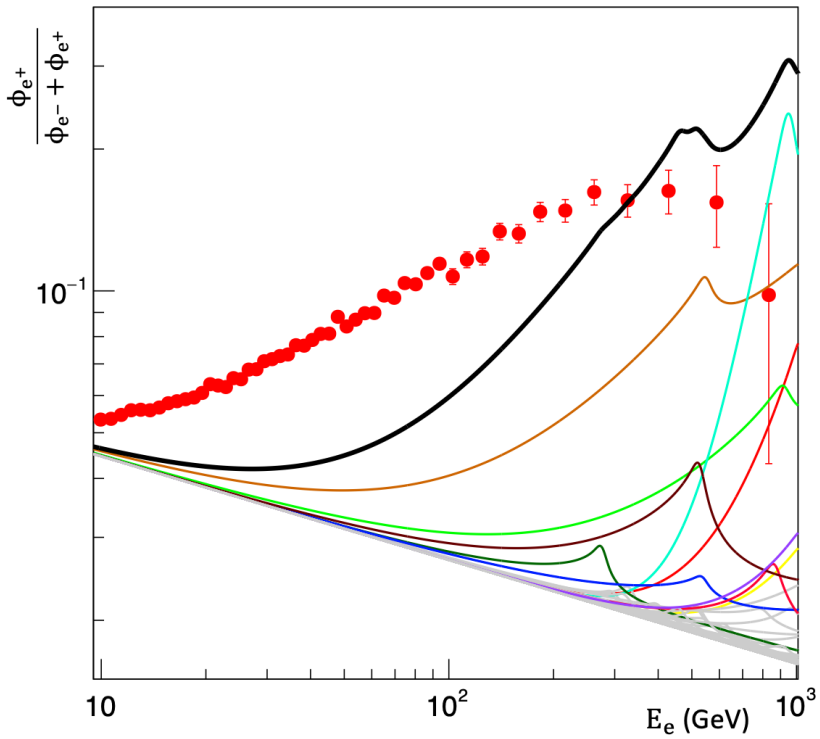

Figure 1. The cosmic-ray positron fraction individually calculated from each of the 103 pulsars in the ATNF catalog that are located within 3 kpc of the Solar System and younger than $\tau_c < 10^6$ years (thin colored lines), and from the sum of all 103 of these sources (thick black line). For the color key, see Table 1. In this figure, we have adopted the following parameters: $\alpha = 1.5$, $E_c = 50\,\mathrm{TeV}$, $\eta = 0.15$, $\tau = 10^4\,\mathrm{yr}$, $B_{\rm ISM} = 3\,\mu\mathrm{G}$, and $t_{\rm PWN} = 3 \times 10^4\,\mathrm{yr}$. For each individual pulsar, we adopt values of τ_c, r, and P as reported in the ATNF catalog.

Pulsar Name	P (s)	d (kpc)	τ_c (yr)	Color (Fig. 1)
J1302-6350	0.048	2.63	3.22×10^5	Light Blue
J1057-5226	0.197	0.093	5.25×10^5	Orange
J0117+5914	0.101	1.77	2.65×10^5	Red
J0633+1746	0.237	0.190	3.32×10^5	Light Green
J2032+4127	0.143	1.33	1.91×10^5	Violet
J0908-4913	0.107	1.00	1.02×10^5	Yellow
J2030+4415	0.227	0.720	5.45×10^5	Brown
J1846+0919	0.226	1.53	3.50×10^5	Pink
J1745-3040	0.367	0.200	5.36×10^5	Blue
J1530-5327	0.279	1.12	9.34×10^5	Green

Table 1. The 10 pulsars contained in the ATNF catalog which contribute the most to the local high-energy cosmic-ray positron flux. For each pulsar, we provide the reported period, distance, and characteristic age. Also given are the colors assigned to each of these pulsars in Fig. 1.

4 Positrons From Unknown Pulsars

A large fraction of the pulsars in the Milky Way, including many young pulsars located near the Solar System, have not yet been detected, and thus are not contained within the ATNF catalog. To estimate the contribution to the cosmic-ray positron flux from these yet-to-be discovered pulsars, we have employed a Monte Carlo with parameters tuned to reproduce the observed characteristics of the ATNF catalog's pulsar population.

For the locations of the pulsars modelled by our Monte Carlos, we draw from the following spatial distribution [23]:

$$n_{\rm pulsar} \propto R^{2.35}\, e^{-R/1530\,{\rm pc}}\, e^{-|z|/300\,{\rm pc}}, \tag{4.1}$$

where R and z describe the location of a given pulsar in cylindrical coordinates (we take the distribution to be symmetric with respect to the angular coordinate). We take the solar system to be located at R= 8.25 kpc and $z = 0$. For the age of each pulsar, we simply draw from a flat distribution.

In the calculations performed by our Monte Carlo, we focus on those pulsars which are located within 3 kpc of the Solar System and that are younger than 10^6 years. While pulsars older than 10^6 years do contribute to the local positron flux, this portion of the spectrum has a negligible degree of variation from realization-to-realization. Consequently, we use an average output from our Monte Carlo to account for the pulsars in this age range. We also find that pulsars located more than 3 kpc from the Solar System contribute negligibly to the local positron flux, at a level that is smaller than the line width used in our plots.

For each realization of our Monte Carlo, we adopt a value for the pulsar birth rate, $R_{\rm PSR}$, as well as for the spindown timescale, τ. For the spatial distribution described by Eq. 4.1, 5.2% of the pulsar population is located within 3 kpc, so in each realization, we simulate a total of $R_{\rm PSR} \times 0.052 \times 10^6 \simeq 520 \times (R_{\rm PSR}/0.01\,{\rm yr}^{-1})$ pulsars [20]. Notice that for reasonable values of $R_{\rm PSR}$, the number of these pulsars is significantly larger than the 103 discussed in the previous section, demonstrating the significant incompleteness of the ATNF catalog.

In order to compare the output of a given Monte Carlo realization to the observed population of young and nearby pulsars, we must establish under what conditions a given pulsar is likely to be detected. In the case of radio detection, the main limiting factor is whether the radio beam is pointed in the direction of the Solar System. To model this, we simply adopt a value for the beaming fraction, $f_{\rm radio}$, which is defined as the probability that a given pulsar produces radio emission in our direction. For this radio emission to be detected, we require both that we reside within the geometry of the radio beam, and that the pulsar's spindown flux is larger than a minimum detectable value, $F_{\rm SD} \equiv \dot{E}/d^2 > F^{\rm min}_{\rm radio}$. In considering the detection of the pulsed gamma-ray emission from pulsars, the corresponding beaming fraction is significantly larger, $f_\gamma > f_{\rm radio}$. In this case, however, Fermi is generally only able to detect those pulsars with a relatively high spindown flux, corresponding to $F^{\rm min}_\gamma > F^{\rm min}_{\rm radio}$.

In Fig. 2, we show an example of one realization of our Monte Carlo, plotting the spin-down flux and age of each detectable pulsar. In this figure, we have adopted the following parameters: $\tau = 10^4\,{\rm yr}$, $P_0 = 0.042\,{\rm s}$, $R_{\rm PSR} = 0.01\,{\rm yr}^{-1}$, $f_{\rm radio} = 0.28$, $f_\gamma = 0.62$, $F^{\rm min}_\gamma = 4.22 \times 10^{42}\,{\rm erg/kpc^2/yr}$, and $F^{\rm min}_{\rm radio} = 2.66 \times 10^{41}\,{\rm erg/kpc^2/yr}$. The symbols used indicate whether a given pulsar is deemed to be detectable by their radio or gamma-ray emission.

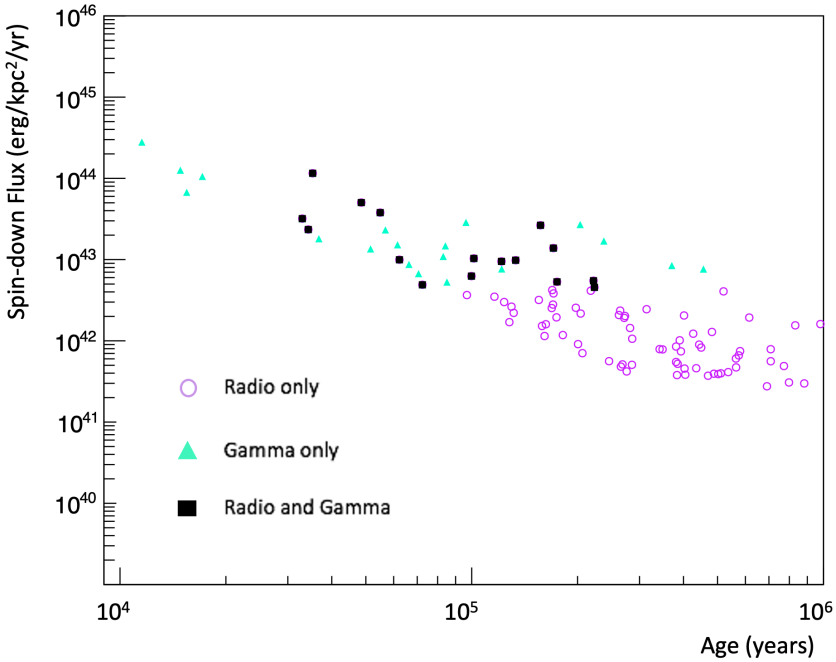

Figure 2. An example of one realization of our Monte Carlo, showing the spin-down flux and age of each detectable pulsar. In this figure, we have adopted the following parameters: $\tau = 10^4\,\mathrm{yr}$, $P_0 = 0.042\,\mathrm{s}$, $R_{\rm PSR} = 0.01\,\mathrm{yr}^{-1}$, $f_{\rm radio} = 0.28$, $f_\gamma = 0.62$, $F_\gamma^{\rm min} = 4.22 \times 10^{42}\,\mathrm{erg/kpc^2/yr}$, and $F_{\rm radio}^{\rm min} = 2.66 \times 10^{41}\,\mathrm{erg/kpc^2/yr}$. The symbols used reflect whether a given pulsar is detectable by their radio or gamma-ray emission.

To constrain the values of f_γ, $f_{\rm radio}$, $F_\gamma^{\rm min}$, and $F_{\rm radio}^{\rm min}$, we compare the observed distribution of detected pulsar ages to the predictions of our Monte Carlo for various combinations of parameter values. These distributions are shown in Fig. 3 for the case of $\tau = 10^4\,\mathrm{yr}$ and $R_{\rm PSR} = 0.01\,\mathrm{yr}^{-1}$, using the best-fit parameter values of $F_\gamma^{\rm min} = 4.22 \times 10^{42}$ ergs/kpc^2/yr, $F_{\rm radio}^{\rm min} = 2.66 \times 10^{42}$ ergs/kpc^2/yr, $f_\gamma = 0.62$, and $f_{\rm radio} = 0.28$. The histograms in these figures represent the number of pulsars detected by Fermi (left frame) and by radio telescopes (right frame), which are then compared to the results of our Monte Carlo, averaged over 1000 realizations. For each choice of parameters, we calculate the Poisson likelihood of obtaining a distribution of pulsars (in terms of age, and in the three distance increments shown) that is consistent with the measured histograms. After repeating this exercise for various parameter values, we identify the best-fit values of $F_\gamma^{\rm min}$, $F_{\rm radio}^{\rm min}$, f_γ, and $f_{\rm radio}$ for each value of τ and $R_{\rm PRB}$ as given in Table 2. Throughout the remainder of our analysis, we will adopt the best-fit values of $F_\gamma^{\rm min}$, $F_{\rm radio}^{\rm min}$, f_γ, and $f_{\rm radio}$ for any given choice of τ and $R_{\rm PRB}$.

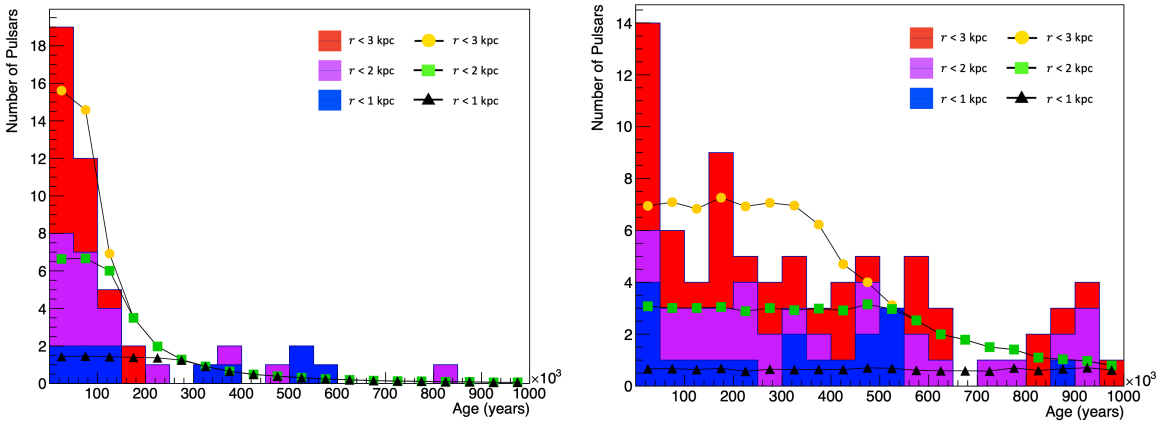

Figure 3. The distribution of ATNF pulsars detected in gamma-rays (left) and in radio emission (right), according to their age and distance from Earth. The curves represent the distributions predicted by our Monte Carlo, averaged over 1000 realizations, for the case of $\tau = 10^4\,\mathrm{yr}$, $R_{\rm PSR} = 0.01\,\mathrm{yr}^{-1}$, $F_\gamma^{\rm min} = 4.22 \times 10^{42}$ ergs/kpc^2/yr, $F_{\rm radio}^{\rm min} = 2.66 \times 10^{42}$ ergs/kpc^2/yr, $f_\gamma = 0.62$, and $f_{\rm radio} = 0.28$.

τ (yr)	$F_\gamma^{\rm min}$ (erg/kpc^2/yr)	f_γ	$F_{\rm radio}^{\rm min}$ (erg/kpc^2/yr)	$f_{\rm radio}$
5×10^3	2.37×10^{42}	0.63	1.33×10^{41}	0.27
1×10^4	4.22×10^{42}	0.62	2.66×10^{41}	0.28
2×10^4	9.44×10^{43}	0.63	3.98×10^{42}	0.26

Table 2. The best-fit values of $F_\gamma^{\rm min}$, $F_{\rm radio}^{\rm min}$, f_γ, and $f_{\rm radio}$ for three values of τ, and for $R_{\rm PSR} = 0.01$ yr^{-1}.

In Fig. 4, we show the cosmic-ray positron fraction from the pulsars in the ATNF catalog, from unknown pulsars as calculated by our Monte Carlo, and from the sum of these contributions, adopting the best-fit values of $F_\gamma^{\rm min}$, $F_{\rm radio}^{\rm min}$, f_γ, and $f_{\rm radio}$ and otherwise using the same parameters as adopted in the previous section. In the following section, we will consideration variations of these parameters and assess their impact on our results.

5 Parameter Variations

The results shown in Fig. 4 were obtained using our default set of parameter values: $\alpha = 1.5$, $E_c = 50\,\mathrm{TeV}$, $t_{\rm PWN} = 3 \times 10^4\,\mathrm{yr}$, $\tau = 10^4\,\mathrm{yr}$, $B = 3\,\mu\mathrm{G}$, and $\eta = 0.15$. Any changes to these parameters will impact the predicted magnitude and spectral shape of the cosmic-ray positron fraction. In this section, we explore these variations and their connection to the observed features of the positron fraction.

In Fig. 5, we illustrate the impact of a variety of parameter variations, modifying one of the above mentioned parameters at a time while keeping the others fixed to their default values (with the exception of η, which is selected in each case to normalize the positron fraction to its measured value at $E_e = 20\,\mathrm{GeV}$). Focusing first on the positron fraction as measured at energies below a few hundred GeV, the positrons in this energy range arise from many pulsars, and thus the positron fraction is largely insensitive to the location, age, or other characteristics of any specific pulsars. From this data, it is clear that an injected

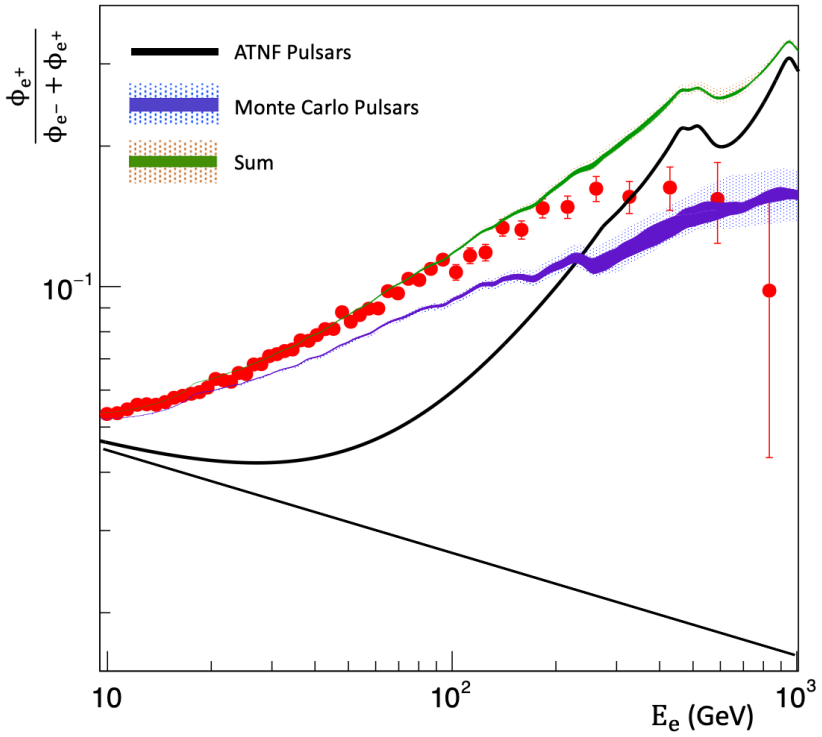

Figure 4. The cosmic-ray positron fraction from the pulsars in the ATNF catalog (black), from unknown pulsars as calculated by our Monte Carlo (blue), and from the sum of these contributions (orange). In this figure, we have adopted the following parameters: $\alpha = 1.5$, $E_c = 50\,\mathrm{TeV}$, $\eta = 0.15$, $\tau = 10^4\,\mathrm{yr}$, $B_{\rm ISM} = 3\,\mu\mathrm{G}$, and $t_{\rm PWN} = 3 \times 10^4\,\mathrm{yr}$, and values of τ_c, r, and P as reported in the ATNF catalog. The solid (shaded) bands around the blue and orange curves reflect the variation observed across 68% (all) of the realizations of our Monte Carlo.

spectral index of approximately $\alpha \sim 1.5 - 1.6$ is preferred, although the precise value of this parameter also depends on the choices of $t_{\rm PWN}$, τ, and B that are adopted. For some choices of these parameters (such as $B = 6\,\mu\mathrm{G}$, for example), the shape of the predicted positron spectrum is more concave than is measured by AMS-02, leading us to disfavor such scenarios.

In some cases, there are substantial degeneracies between the parameters we have considered. In particular, we find that the value of the injected cutoff energy, E_c, is approximately degenerate with the electron-positron production efficiency, η. This is demonstrated in the upper right frame of Fig. 5, where we show that the low-energy positron fraction is not significantly impacted by variations in E_c, other than in terms of the overall normalization. If we increase the value of E_c, we must compensate by increasing the value of the efficiency, η.

Upon reviewing these results, one might reasonably be concerned that when we select model parameters which provide a good fit to the positron fraction at low energies, we consistently predict a positron flux at high energies that is larger than that observed by AMS-02. This could be an indication that some young pulsars lose their kinetic energy more rapidly than we have assumed (in this study, we have limited our calculations to the case of magnetic dipole breaking). Furthermore, in light of the fact that the positron fraction is dominated at the highest measured energies by only a small number of sources, this could simply be the consequence of a small number of young and nearby pulsars which have characteristics

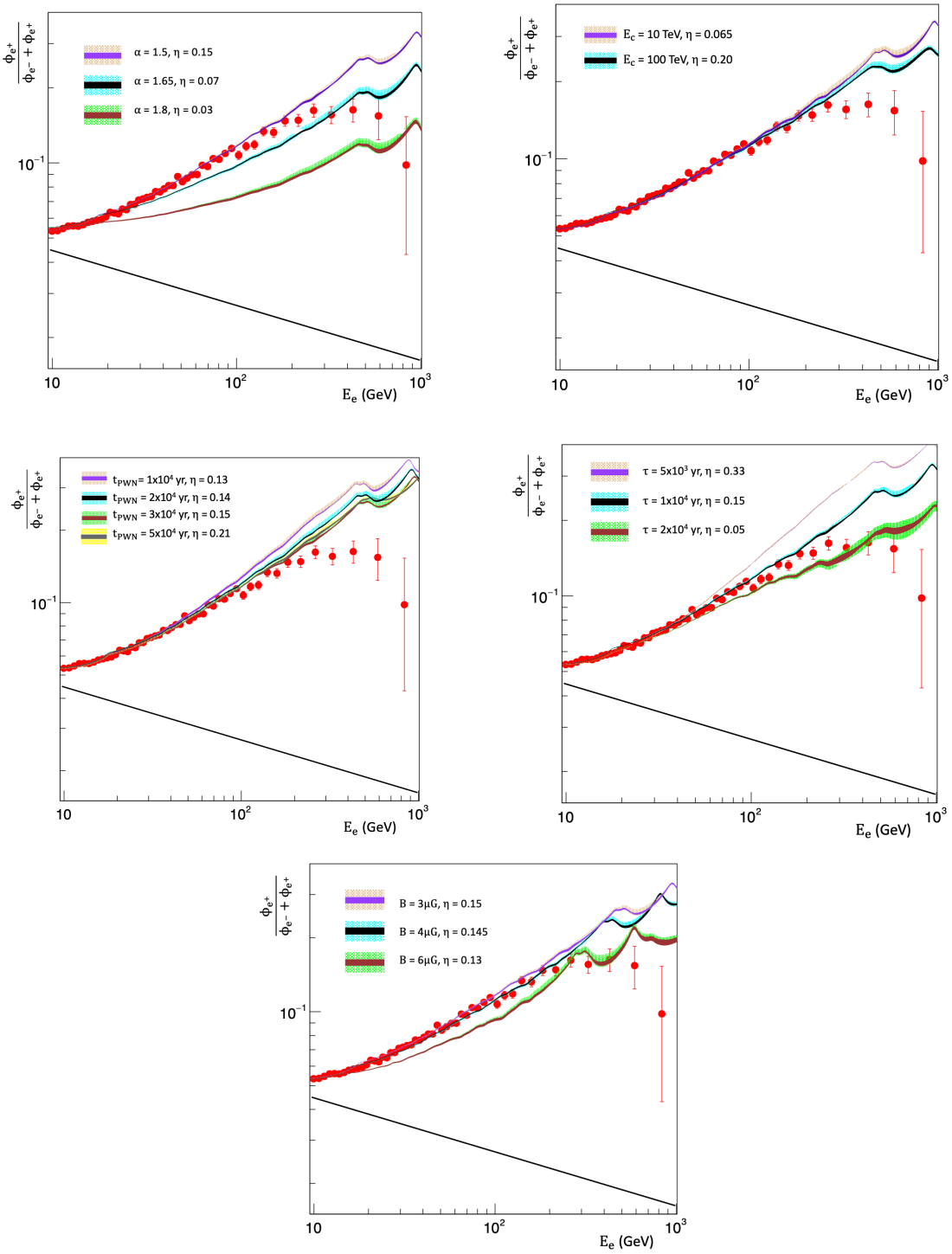

Figure 5. The impact on the positron fraction of varying the injected spectral index, α, the injected spectral cutoff, E_c, the duration of the pulsars wind nebula phase, $t_{\rm PWN}$, the spindown timescale, τ, or the magnetic field of the ISM, B.

that are substantially different from the average of the local population. We will explore this possibility further in the following section.

6 Pulsar-to-Pulsar Variations

Throughout this study, we have adopted parameter values which are intended to reflect the average characteristics of the local pulsar population. At low and moderate energies, we can expect this approach to be adequate, as the observed positron fraction is the result of non-negligible contributions from several dozen individual pulsars. At higher energies, however, the measured positron fraction could potentially be dominated by the emission from only a few individual pulsars. Judging from Fig. 1, for example, the single most important pulsar (PSR J1057-5226) contributes less than 15% of the observed positrons at 100 GeV, but is responsible for producing roughly half of these particles at 500 GeV. The specific parameters for this individual pulsar are thus quite important for our prediction of the positron fraction at high energies. More generally speaking, stochastic variations in the parameters of individual pulsars make it difficult to reliably predict the positron fraction at energies above a few hundred GeV. It is, after all, very plausible that the pulsar parameters being considered in this study are not universal, but rather vary significantly from pulsar-to-pulsar.

We explore some examples of the possible impact of pulsar-to-pulsar variations in Fig. 6 where we show the positron fraction for the case of $\alpha = 1.55$ (top) or 1.50 (bottom), $E_c = 10\,\text{TeV}$, $t_{\text{PWN}} = 5 \times 10^4\,\text{yr}$, $\tau = 10^4\,\text{yr}$ and $B = 4\,\mu\text{G}$. In each frame, we show the positron spectrum that results when we include all of the pulsars (both those in the ATNF catalog, and those simulated by our Monte Carlo), as well as that obtained when we neglect the contributions from the first four pulsars listed in Table 1. At low to moderate energies, these few pulsars do not impact the positron fraction much, and we consistently obtain a result which is in reasonably good agreement with the measured spectrum. At energies above a few hundred GeV, in contrast, the result changes significantly depending on the detailed properties of these few individual pulsars. This makes it impossible for us to use our approach to reliably predict the positron fraction at the highest energies measured by AMS-02.

7 Summary and Conclusions

Observations by the HAWC Collaboration indicate that pulsars are accompanied by TeV halos which produce a significant contribution to the cosmic-ray positron flux. In this study, we have used the measured characteristics of the cosmic-ray positron fraction to constrain the properties of the local population of pulsars and their associated TeV halos. More specifically, we have calculated the contribution to the cosmic-ray positron flux from the pulsars contained within the Australia Telescope National Facility (ATNF) pulsar catalog [24], and used a Monte Carlo to estimate the contribution from those pulsars which have thus far gone undetected. After varying a number of parameters, including the spectral shape of the injected positrons, the timescale for pulsar spindown, the efficiency for electron-positron production, the magnitude of the magnetic field in the ISM, and the duration of the pulsar wind nebula phase, we have compared our results to the positron fraction as measured by AMS-02. For reasonable parameter values, we find that it is possible to obtain good agreement with the measured positron fraction, at least up to energies of $E_e \sim 300\,\text{GeV}$. This result further supports the conclusion that TeV halos are the main source of the observed cosmic-ray positron spectrum. At energies above a few hundred GeV, the positron fraction

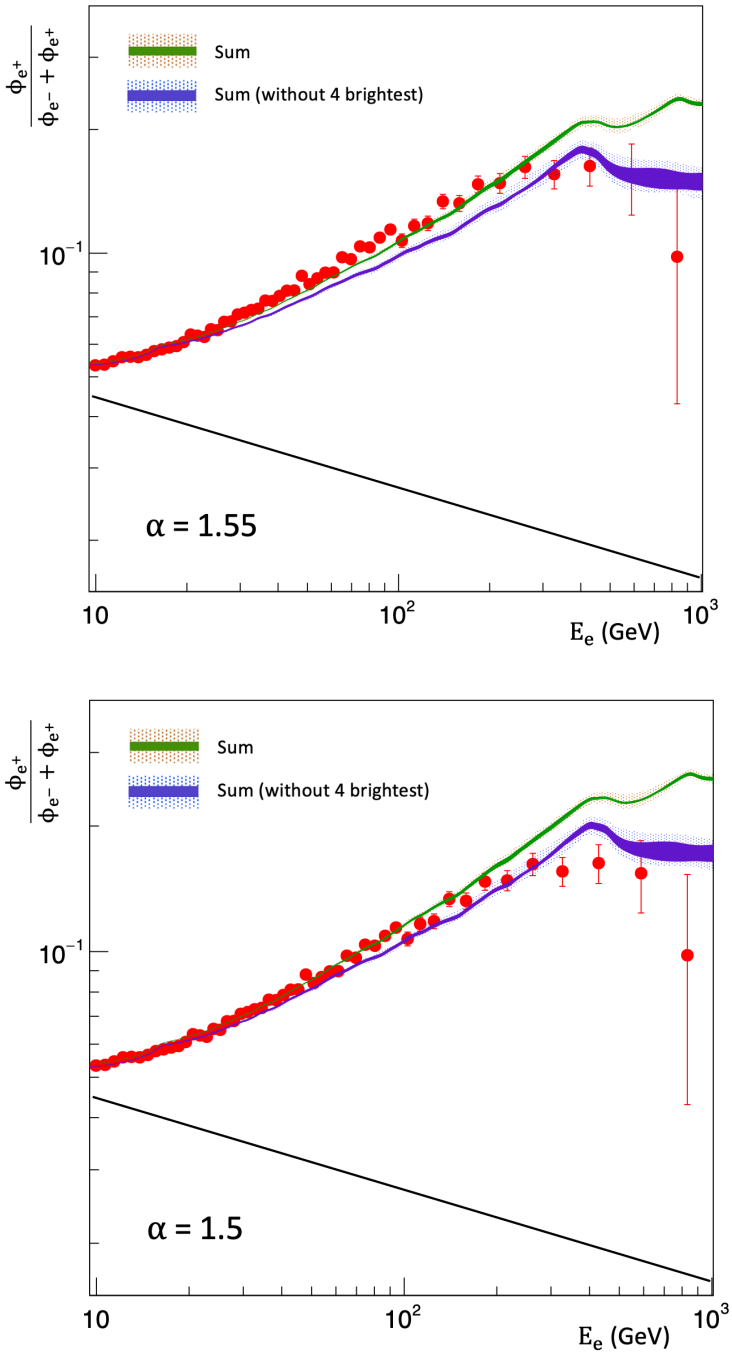

Figure 6. The cosmic-ray positron fraction as calculated for $\alpha = 1.55$ (top) or $\alpha = 1.50$ (bottom), $E_c = 10\,\mathrm{TeV}$, $t_{\mathrm{PWN}} = 5 \times 10^4\,\mathrm{yr}$, $\tau = 10^4\,\mathrm{yr}$ and $B = 4\,\mu\mathrm{G}$. In each frame, we show the positron spectrum that results when we include all of the pulsars (both those in the ATNF catalog, and those simulated by our Monte Carlo), as well as that obtained when we neglect the contributions from the first four pulsars listed in Table 1. This illustrates the importance of pulsar-to-pulsar parameter variations, in particular at energies above a few hundred GeV.

is dominated by a small number of pulsars, limiting our ability to reliably predict the shape of the expected positron fraction or to use this high-energy information to draw reliable conclusions pertaining to the Milky Way's broader pulsar population.

Overall, the observed positron spectrum supports a picture in which pulsars transfer $\eta \sim 5-20\%$ of their total spindown power into the production of high-energy electron-positron pairs, generating a spectrum of such particles with a hard spectral index, $\alpha \sim 1.5-1.7$. Our best fits were obtained for models in which the radio beams of pulsars cover $\sim 28\%$ of the surrounding solid angle, while the gamma-ray beams are significantly wider, covering $\sim 62\%$ of the total solid angle.

Acknowledgments

We would like to thank Tim Linden for helpful discussions. DH is supported by the Fermi Research Alliance, LLC under Contract No. DE-AC02-07CH11359 with the U.S. Department of Energy, Office of Science, Office of High Energy Physics.

References

[1] A. U. Abeysekara et al. "Extended gamma-ray sources around pulsars constrain the origin of the positron flux at Earth". In: *Science* 358.6365 (2017), pp. 911–914. DOI: 10.1126/science.aan4880. arXiv: 1711.06223 [astro-ph.HE].

[2] A. U. Abeysekara et al. "Multiple Galactic Sources with Emission Above 56 TeV Detected by HAWC". In: *Phys. Rev. Lett.* 124.2 (2020), p. 021102. DOI: 10.1103/PhysRevLett.124.021102. arXiv: 1909.08609 [astro-ph.HE].

[3] O. Adriani et al. "Cosmic-Ray Positron Energy Spectrum Measured by PAMELA". In: *Phys. Rev. Lett.* 111 (8 2013), p. 081102. DOI: 10.1103/PhysRevLett.111.081102. URL: https://link.aps.org/doi/10.1103/PhysRevLett.111.081102.

[4] M. Aguilar et al. "Cosmic-ray positron fraction measurement from 1 to 30 GeV with AMS-01". In: *Physics Letters B* 646.4 (2007), 145–154. ISSN: 0370-2693. DOI: 10.1016/j.physletb.2007.01.024. URL: http://dx.doi.org/10.1016/j.physletb.2007.01.024.

[5] M. Aguilar et al. "Towards Understanding the Origin of Cosmic-Ray Electrons". In: *Phys. Rev. Lett.* 122 (10 2019), p. 101101. DOI: 10.1103/PhysRevLett.122.101101. URL: https://link.aps.org/doi/10.1103/PhysRevLett.122.101101.

[6] M. Aguilar et al. "Towards Understanding the Origin of Cosmic-Ray Positrons". In: *Phys. Rev. Lett.* 122 (4 2019), p. 041102. DOI: 10.1103/PhysRevLett.122.041102. URL: https://link.aps.org/doi/10.1103/PhysRevLett.122.041102.

[7] A. Albert et al. "3HWC: The Third HAWC Catalog of Very-High-Energy Gamma-ray Sources". In: *Astrophys. J.* 905.1 (2020), p. 76. DOI: 10.3847/1538-4357/abc2d8. arXiv: 2007.08582 [astro-ph.HE].

[8] A. Albert et al. "Evidence that Ultra-high-energy Gamma Rays Are a Universal Feature near Powerful Pulsars". In: *Astrophys. J. Lett.* 911.2 (2021), p. L27. DOI: 10.3847/2041-8213/abf4dc. arXiv: 2101.07895 [astro-ph.HE].

[9] S. W. Barwick et al. "Measurements of the Cosmic-Ray Positron Fraction from 1 to 50 G[CLC]e[/CLC]V". In: *The Astrophysical Journal* 482.2 (1997), L191–L194. ISSN: 0004-637X. DOI: 10.1086/310706. URL: http://dx.doi.org/10.1086/310706.

[10] Pasquale Blasi. "Origin of the Positron Excess in Cosmic Rays". In: *Physical Review Letters* 103.5 (2009). ISSN: 1079-7114. DOI: 10.1103/physrevlett.103.051104. URL: http://dx.doi.org/10.1103/PhysRevLett.103.051104.

[11] Ilias Cholis, Tanvi Karwal, and Marc Kamionkowski. "Features in the Spectrum of Cosmic-Ray Positrons from Pulsars". In: *Phys. Rev. D* 97.12 (2018), p. 123011. DOI: 10.1103/PhysRevD.97.123011. arXiv: 1712.00011 [astro-ph.HE].

[12] Ilias Cholis, Tanvi Karwal, and Marc Kamionkowski. "Studying the Milky Way pulsar population with cosmic-ray leptons". In: *Phys. Rev. D* 98.6 (2018), p. 063008. DOI: 10.1103/PhysRevD.98.063008. arXiv: 1807.05230 [astro-ph.HE].

[13] V. Di Felice et al. "Looking for cosmic ray data? The ASI Cosmic Ray Database". In: *35th International Cosmic Ray Conference (ICRC2017)*. Vol. 301. International Cosmic Ray Conference. Jan. 2017, 1073, p. 1073.

[14] Kun Fang, Xiao-Jun Bi, and Peng-fei Yin. "Discriminating local sources of high-energy cosmic electrons and positrons by current and future anisotropy measurements". In: *Mon. Not. Roy. Astron. Soc.* 478.4 (2018), pp. 5660–5670. DOI: 10.1093/mnras/sty1463. arXiv: 1706.03745 [astro-ph.HE].

[15] Dan Hooper and Tim Linden. "Evidence of TeV Halos Around Millisecond Pulsars". In: (Mar. 2021). arXiv: 2104.00014 [astro-ph.HE].

[16] Dan Hooper and Tim Linden. "Measuring the local diffusion coefficient with H.E.S.S. observations of very high-energy electrons". In: *Physical Review D* 98.8 (2018). ISSN: 2470-0029. DOI: 10.1103/physrevd.98.083009. URL: http://dx.doi.org/10.1103/PhysRevD.98.083009.

[17] Dan Hooper and Tim Linden. "Measuring the Local Diffusion Coefficient with H.E.S.S. Observations of Very High-Energy Electrons". In: *Phys. Rev. D* 98.8 (2018), p. 083009. DOI: 10.1103/PhysRevD.98.083009. arXiv: 1711.07482 [astro-ph.HE].

[18] Dan Hooper and Tim Linden. "Millisecond Pulsars, TeV Halos, and Implications For The Galactic Center Gamma-Ray Excess". In: *Phys. Rev. D* 98.4 (2018), p. 043005. DOI: 10.1103/PhysRevD.98.043005. arXiv: 1803.08046 [astro-ph.HE].

[19] Dan Hooper et al. "HAWC observations strongly favor pulsar interpretations of the cosmic-ray positron excess". In: *Physical Review D* 96.10 (2017). ISSN: 2470-0029. DOI: 10.1103/physrevd.96.103013. URL: http://dx.doi.org/10.1103/PhysRevD.96.103013.

[20] Simon Johnston et al. "The Galactic population and properties of young, highly energetic pulsars". In: *Monthly Notices of the Royal Astronomical Society* 497.2 (2020), 1957–1965. ISSN: 1365-2966. DOI: 10.1093/mnras/staa2110. URL: http://dx.doi.org/10.1093/mnras/staa2110.

[21] Jagdish C. Joshi and Soebur Razzaque. "A self-consistent model of cosmic-ray fluxes and positron excess: Roles of nearby pulsars and a sub-dominant source population". In: *JCAP* 09 (2017), p. 029. DOI: 10.1088/1475-7516/2017/09/029. arXiv: 1706.01981 [astro-ph.HE].

[22] Tim Linden et al. "Using HAWC to discover invisible pulsars". In: *Phys. Rev. D* 96.10 (2017), p. 103016. DOI: 10.1103/PhysRevD.96.103016. arXiv: 1703.09704 [astro-ph.HE].

[23] Dunc R. Lorimer. "The galactic population and birth rate of radio pulsars". In: *IAU Symp.* 218 (2004), p. 105. arXiv: astro-ph/0308501.

[24] R. N. Manchester et al. "The Australia Telescope National Facility Pulsar Catalogue". In: *The Astronomical Journal* 129.4 (2005), 1993–2006. ISSN: 1538-3881. DOI: 10.1086/428488. URL: http://dx.doi.org/10.1086/428488.

[25] I. V. Moskalenko and A. W. Strong. "Production and propagation of cosmic ray positrons and electrons". In: *Astrophys. J.* 493 (1998), pp. 694–707. DOI: 10.1086/305152. arXiv: astro-ph/9710124.

[26] Luca Orusa et al. "Constraining positron emission from pulsar populations with AMS-02 data". In: *JCAP* 12.12 (2021), p. 014. DOI: 10.1088/1475-7516/2021/12/014. arXiv: 2107.06300 [astro-ph.HE].

[27] Stefano Profumo. "Dissecting cosmic-ray electron-positron data with Occam's Razor: the role of known Pulsars". In: *Central Eur. J. Phys.* 10 (2011), pp. 1–31. DOI: 10.2478/s11534-011-0099-z. arXiv: 0812.4457 [astro-ph].

[28] Stefano Profumo et al. "Lessons from HAWC pulsar wind nebulae observations: The diffusion constant is not a constant; pulsars remain the likeliest sources of the anomalous positron fraction; cosmic rays are trapped for long periods of time in pockets of inefficient diffusion". In: *Phys. Rev. D* 97.12 (2018), p. 123008. DOI: 10.1103/PhysRevD.97.123008. arXiv: 1803.09731 [astro-ph.HE].

[29] Takahiro Sudoh, Tim Linden, and Dan Hooper. "The Highest Energy HAWC Sources are Likely Leptonic and Powered by Pulsars". In: (Jan. 2021). DOI: 10.1088/1475-7516/2021/08/010. arXiv: 2101.11026 [astro-ph.HE].

[30] V. Vagelli. "Results from AMS-02 on the ISS after 6 years in space". In: *Nuovo Cim. C* 42.4 (2019), p. 173. DOI: 10.1393/ncc/i2019-19173-y.

[31] Andrey E. Vladimirov et al. "GALPROP WebRun: an internet-based service for calculating galactic cosmic ray propagation and associated photon emissions". In: *Comput. Phys. Commun.* 182 (2011), pp. 1156–1161. DOI: 10.1016/j.cpc.2011.01.017. arXiv: 1008.3642 [astro-ph.HE].